

Anisotropic Finite-Size Scaling Analysis of a Two-Dimensional Driven Diffusive System

Jian-Sheng Wang*

The two-dimensional uniformly driven diffusive system is simulated with a multi-spin coding technique. The nonequilibrium phase transition is analyzed with anisotropic finite-size scaling, both at the critical point and off the critical point. The field-theoretical values of critical exponents fit the data well.

Key Words: Driven diffusive systems; anisotropic finite-size scaling; nonequilibrium phase transitions; computer simulations.

1. Introduction

Driven diffusive systems are a class of models which exhibit nonequilibrium phase transitions.⁽¹⁻⁴⁾ The models are defined by some local rules similar to Kawasaki dynamics. The steady states of the dynamical evolution have been studied extensively during past decade. A central issue is whether the concept of universality of critical phenomena can be applied in nonequilibrium cases.

The standard driven diffusive model of half-filled charged lattice gas was proposed as a model for ionic solution in an electric field.^(1,2) A continuum version, based on symmetries and conservation laws, was solved in a field-theoretic framework.^(5,6) It is quite remarkable that exact critical exponents are obtained for dimensions from two to five. In particular, the set of critical exponents in two dimensions is

$$\beta = \frac{1}{2}, \quad \gamma = 1, \quad \nu_{\parallel} = \frac{3}{2}, \quad \nu_{\perp} = \frac{1}{2}. \quad (1)$$

These exponents have similar meanings as in equilibrium second-order phase transitions. They are thought to be universal within a class. No independent methods have

* Computational Science, Blk S16, National University of Singapore, Lower Kent Ridge Road, Singapore 0511. E-mail: cscwjs@leonis.nus.sg

been applied to the problem to check out the validity of the claim except computer simulations.^(7,8) Anisotropic finite-size scaling studies by Leung^(9,10) appear to have settled a dispute between theory and early computer simulations. But a recent work⁽⁸⁾ casts doubt on Leung's conclusion. We present here high quality data to support Leung's results.

2. Model and Simulation

The system consists of a square lattice of $L \times M$ sites. The driven field is in x direction. A configuration is specified by a set of Ising spins, $\sigma_{x,y} = \pm 1$, with zero total magnetization. The state evolves according to the following prescription. A bond is chosen with equal probability in orientations and in locations. If the bond is parallel to the driven field and the adjoining spins are distinct, the spins are changed to $\sigma_{x,y} = -1$ and $\sigma_{x+1 \bmod L,y} = +1$. This corresponds to an infinitely strong driven field. If the bond is perpendicular to the field, we swap the spin values with a probability $\min\{1, \exp(-\delta E/k_B T)\}$, where δE is the energy increment due to the change, assuming the usual nearest neighbor ferromagnetic interaction with coupling constant J and periodic boundary conditions. One Monte Carlo step is defined as $L \times M$ such basic steps.

Simulation near critical point is not easy because of critical slowing down. The situation for this model is more severe by the conservative nature of the dynamics, leading to relaxation time $\tau \propto M^4$. Thus, an efficient implementation is crucial to obtain good statistics. With a multi-spin coding method,⁽¹¹⁾ thirty two systems are simulated simultaneously. This gives us at least a factor of 10 speed up. A slight penalty of the multi-spin coding algorithm is that the temperature can not be set exactly to the desired value. But it can be well under control with a large random bit table. To achieve an accuracy of five significant figures, we took a random bit table of 2^{18} entries.

The program runs at 0.3 μ sec per spin exchange on an SGI Iris Indigo Workstation. Computations were done on a cluster of over fifty workstations (SGI Iris Indigo, HP 9000/700 model 712, and DEC 5000) in two months. The lengths of the runs are 10^7

to 10^8 Monte Carlo steps. These are orders of magnitude longer than previous studies. Measurements are performed at an interval of 10 Monte Carlo steps.

We use the order parameter introduced by Binder and Wang⁽¹²⁾ and modified by Leung.⁽⁹⁾ Let's define

$$\phi = \frac{1}{2L} \sin\left(\frac{\pi}{M}\right) \left| \sum_{x=0}^{L-1} \sum_{y=0}^{M-1} \sigma_{x,y} e^{i2\pi y/M} \right|. \quad (2)$$

The normalization is such that $\phi = 1$ for a strip geometry (the configuration in the limit $T \rightarrow 0$). The following quantities are calculated, (1) the order parameter $\Psi = \langle \phi \rangle$, (2) the ‘‘susceptibility,’’ or fluctuation of the order parameter,

$$\chi = \frac{2L}{\sin \pi/M} \left[\langle \phi^2 \rangle - \langle \phi \rangle^2 \right], \quad (3)$$

and the susceptibility above the critical temperature,

$$\chi' = \frac{2L}{\sin \pi/M} \langle \phi^2 \rangle, \quad (4)$$

and (3) the fourth-order cumulant,

$$g = 2 - \frac{\langle \phi^4 \rangle}{\langle \phi^2 \rangle^2}. \quad (5)$$

Note that g goes from 0 to 1 as temperature T goes from ∞ to 0. We'll measure temperature in units of the two-dimensional Ising critical temperature ($2.269J/k_B$).

3. Determination of the Critical Temperature

Estimating the critical exponents depends crucially on an accurate value of critical temperature. In the literature different authors have given incompatible values, $T_c = 1.355 \pm 0.003$ by Vallés and Marro,⁽⁷⁾ $T_c = 1.30 \pm 0.01$ by Achahbar and Marro,⁽⁸⁾ and Leung's result⁽⁹⁾ of $T_c = 1.418 \pm 0.005$. The discrepancies are the manifestation of the difficulties of simulating the system and of interpreting the complicated finite-size data.

We determine T_c using two independent methods. First, we look at the peak of the susceptibility χ . The method is not particularly accurate, but we get a general picture of the finite-size critical temperature $T_c(L, M)$. For very elongated shapes, $T_c(L, M)$

decreases towards zero. For a fixed value M or L , $T_c(L, M)$ reaches its maximum at about $S = L^{1/3}/M \approx 0.2$. The systems with ratio $S \approx 0.2$ notice the finiteness of the sizes in two directions at roughly the same temperature. $T_c(L, M)$ increases as system size increases with fixed S . Figure 1 is a plot of the peak locations $T_c(L, M)$ versus $L^{-2/3}$, for some fixed values S as well as for the square geometry $L = M$. According to the usual finite-size scaling assumption, we should expect

$$T_c(L, M) = T_c(\infty, \infty) + F(S)L^{-1/\nu_{\parallel}}. \quad (6)$$

Clearly, the data do not follow this equation very well, presumably due to corrections to scaling. But linear extrapolations should give us lower bounds for the infinite system transition temperature T_c . We quote the following result,

$$T_c = 1.410 \pm 0.006. \quad (7)$$

It agrees with Leung's result⁽⁹⁾ within errors. For the square systems, the convergence to the critical temperature is extremely slow. This may explain why the previous calculations on square systems all gave a lower T_c . If anisotropy is a dominant feature, we should not expect peak locations to scale simply as $L^{-1/\nu}$ for square systems.

The peaks were not located with great precise because the simulations were carried out at discrete points spaced at $\Delta T = 0.01$. The second method exploits the scaling properties of the fourth-order cumulant. From finite-size scaling theory, we have

$$g(T, L, M) = \tilde{g}(L^{1/\nu_{\parallel}}(T - T_c)/T_c, S). \quad (8)$$

If scaling were exactly obeyed, different curves (with fixed S) should intersect at exactly the same value T_c . Therefore, there is no need to extrapolate to infinite size. In practice there are unknown corrections to scaling. A better way is to consider the overall scaling, Eq. 8. The value of T_c for each S can be determined more precisely. However, there are weak size and S dependence. Nevertheless, we found that the values all fall into the interval 1.395 to 1.410. Figure 2 is one of the scaling plots with $S = 2^{-8/3}$.

Even with much greater computational effort, the accuracy of T_c has not been improved. Each set of data or each method may give more accurate value, but different sets of data or methods give slightly different values.

4. Anisotropic Finite-Size Scaling at Critical Point

The finite-size scaling theory of isotropic systems can be generalized to anisotropic systems.⁽¹²⁾ The idea is that the anisotropic system has the same scaling form as the isotropic one if we fix the ratio $S = L^{\nu_{\perp}/\nu_{\parallel}}/M$. In anisotropic finite-size scaling, S enters as an independent variable, in addition to the usual scaling variable $L^{1/\nu_{\parallel}}(T - T_c)/T_c$. particularly, at $T = T_c$, scaling functions depend on S .

In applying the finite-size scaling theory, we could simulate a very large system and study the size effect of smaller subsystems. This may seem computationally effective. But there are two problems associated with it: we have the annoying finite-size effect of the very large system when the subsystem sizes are comparable to it; and we may not be able to equilibrate the very large system very well. So, we adopt the more conventional finite-size scaling analysis—working on fully finite size of dimension $L \times M$.

The exponent ratio $\nu_{\parallel}/\nu_{\perp}$ is one of the most important number in an anisotropic finite-size analysis. Theoretical result is often assumed.^(9,13) We have attempted to determine it from our data. The strip geometry with $S \rightarrow 0$ or $S \rightarrow \infty$ and periodic boundary conditions has a simpler scaling behavior at the critical temperature,⁽¹²⁾

$$\chi(T_c) \propto M^{\gamma/\nu_{\perp}}, \quad \Psi(T_c) \propto M^{\gamma/2\nu_{\perp}-1/2}L^{-1/2}, \quad L \gg M^{\nu_{\parallel}/\nu_{\perp}}, \quad (9)$$

$$\chi(T_c) \propto L^{\gamma/\nu_{\parallel}}, \quad \Psi(T_c) \propto L^{\gamma/2\nu_{\parallel}-1/2}M^{-1/2}, \quad M \gg L^{\nu_{\perp}/\nu_{\parallel}}. \quad (10)$$

Figure 3 shows the long strip limiting behavior for the order parameter. The slopes are $\gamma/(2\nu_{\perp})$ and $\gamma/(2\nu_{\parallel})$, respectively. The large L limit is easily achieved, obtaining $\gamma/(2\nu_{\perp}) = 0.96 \pm 0.03$, in accordance with theory. The other limit is hard to reach, because of the slow relaxation in transverse direction. In any case, we found $\gamma/(2\nu_{\parallel}) = 0.37 \pm 0.04$.

The order parameter or susceptibility at T_c has an extra factor which depends on the ratio S , e.g.,

$$\Psi(T_c, L, M) = M^{-\beta/\nu_{\perp}} \tilde{\Psi}(L^{\nu_{\perp}/\nu_{\parallel}}/M). \quad (11)$$

Moreover, the scaling function obeys $\tilde{\Psi}(S) \rightarrow S^{-\nu_{\parallel}/(2\nu_{\perp})}$ for $S \rightarrow \infty$, and $\tilde{\Psi}(S) \rightarrow S^{1/2-\beta/\nu_{\perp}}$ for $S \rightarrow 0$, as a consequence of the limiting behaviors for very long strips

[Eq. (9) and (10)] and the hyperscaling relation

$$2\beta + \gamma = \nu_{\perp} + \nu_{\parallel}. \quad (12)$$

The scaling form was tested for Ising model.⁽¹²⁾ Previous applications to anisotropic systems were not very successful.^(8,14) Figure 4 is a scaling plot with theoretical values of exponents and $T_c = 1.41$. Similar plots for $T = 1.40$ and 1.42 show definite deviations from scaling. This supports our choice of T_c . The asymptotic slopes for small and large scaling variable $S = L^{1/3}/M$ are consistent with the expected value $-1/2$ and $-3/2$, respectively.

In Fig. 5 we plot similarly the susceptibility at $T_c = 1.41$ in scaling form. The asymptotic scaling behavior is borne out,

$$\chi(T_c, L, M) = M^{\gamma/\nu_{\perp}} \tilde{\chi}(L^{\nu_{\perp}/\nu_{\parallel}}/M). \quad (13)$$

The scaling function $\tilde{\chi}(S)$ for large S is $\tilde{\chi}(S) \rightarrow const$, and for $S \rightarrow 0$ we have $\tilde{\chi}(S) \rightarrow S^{\gamma/\nu_{\perp}}$. The data are in full accord with expectations.

Figure 6 is the scaling plot for the fourth-order cumulant,

$$g(T_c, L, M) = \tilde{g}(L^{\nu_{\perp}/\nu_{\parallel}}/M). \quad (14)$$

Large finite-size corrections are found here. This is also the case for the Ising model.⁽¹²⁾

These scaling plots are good evidence that at least the exponent ratios β/ν_{\perp} and $\nu_{\parallel}/\nu_{\perp}$ are in agreement with the field-theoretic values. Scaling off the critical temperature will determine the exponents themselves.

5. Anisotropic Scaling away from Critical Temperature

We expect when $T \neq T_c$,

$$\Psi(T, L, M) = L^{-\beta/\nu_{\parallel}} \tilde{\Phi}(L^{1/\nu_{\parallel}}(T - T_c)/T_c, S), \quad (15)$$

Leung⁽⁹⁾ proposed a stronger scaling form when $S \rightarrow 0$. Figure 7 is a scaling plot of the order parameter for $S = 2^{-8/3}$ with $T_c = 1.41$, assuming the field-theoretical

exponents $\beta = 1/2$, $\nu_{\perp} = 1/2$, and $\nu_{\parallel} = 3/2$. The $T > T_c$ branch (lower part) obeys scaling very well. For the $T < T_c$ branch (upper part), deviation from scaling is large. It appears that the scaling region for $T < T_c$ is rather narrow. The size effect is further complicated by a $1/M$ correction due to the presence of interfaces below T_c . It is also not known how much of this can be attributed to possible logarithmic corrections to scaling. Comparing with Leung's data,^(9,10) we feel that his conclusion on data collapse is somewhat too optimistic.

Our 1024×64 order parameter data can be compatible with the exponent $\beta = 1/2$, but only in a rather narrow critical region of $\Delta T = 0.05$ (see Fig. 8). The data can be fitted to a power $\beta \approx 0.3$ in a large temperature region ($\Delta T = 0.2$). This is also roughly the value found in previous work on square geometry.^(7,8) However, the evidence for $\beta \approx 0.3$ is not convincing since the extrapolated critical temperature would be too low.

Figure 9 is a scaling plot for the susceptibility, χ' , above the critical temperature. Good data collapse is obtained with the theoretical exponents. The asymptotic slope for large scaling variable $M^2(T - T_c)/T_c$ is approximately $\gamma \approx 1$. We should not worry about the deviations from scaling for large values of $T - T_c$. Just like the order parameter, the data below the critical temperature (not shown here) don't scale well.

6. Conclusion

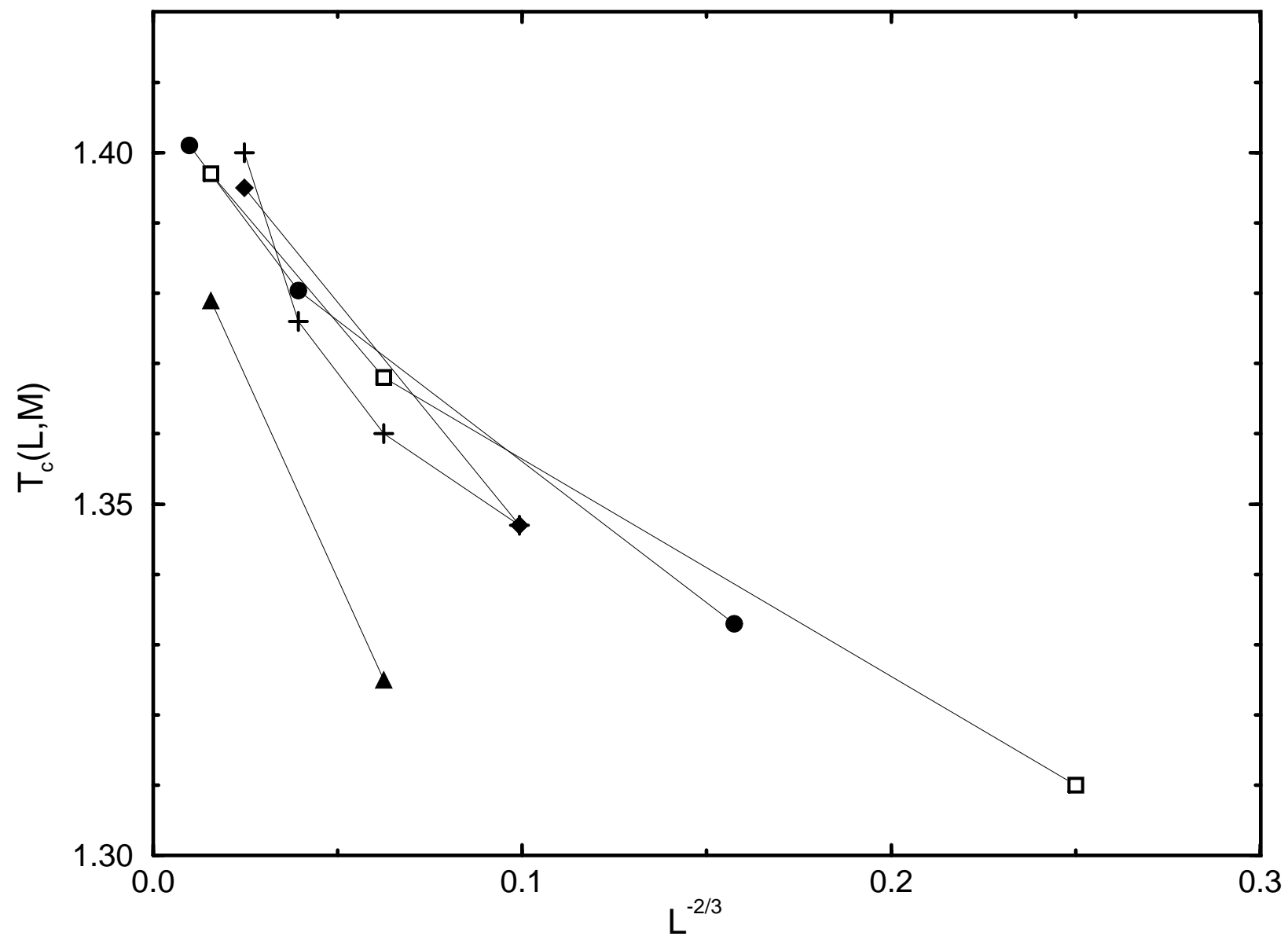
Extensive computer simulation of the driven diffusive model is performed. The new data are consistent with the phenomenological finite-size scaling theory with the set of exponents derived from field-theoretic model. Thus, this work supports the concept of universality of the critical exponents. The order parameter data below the critical temperature are somewhat difficult to interpret. The data at and above the critical temperature conform to standard finite-size scaling.

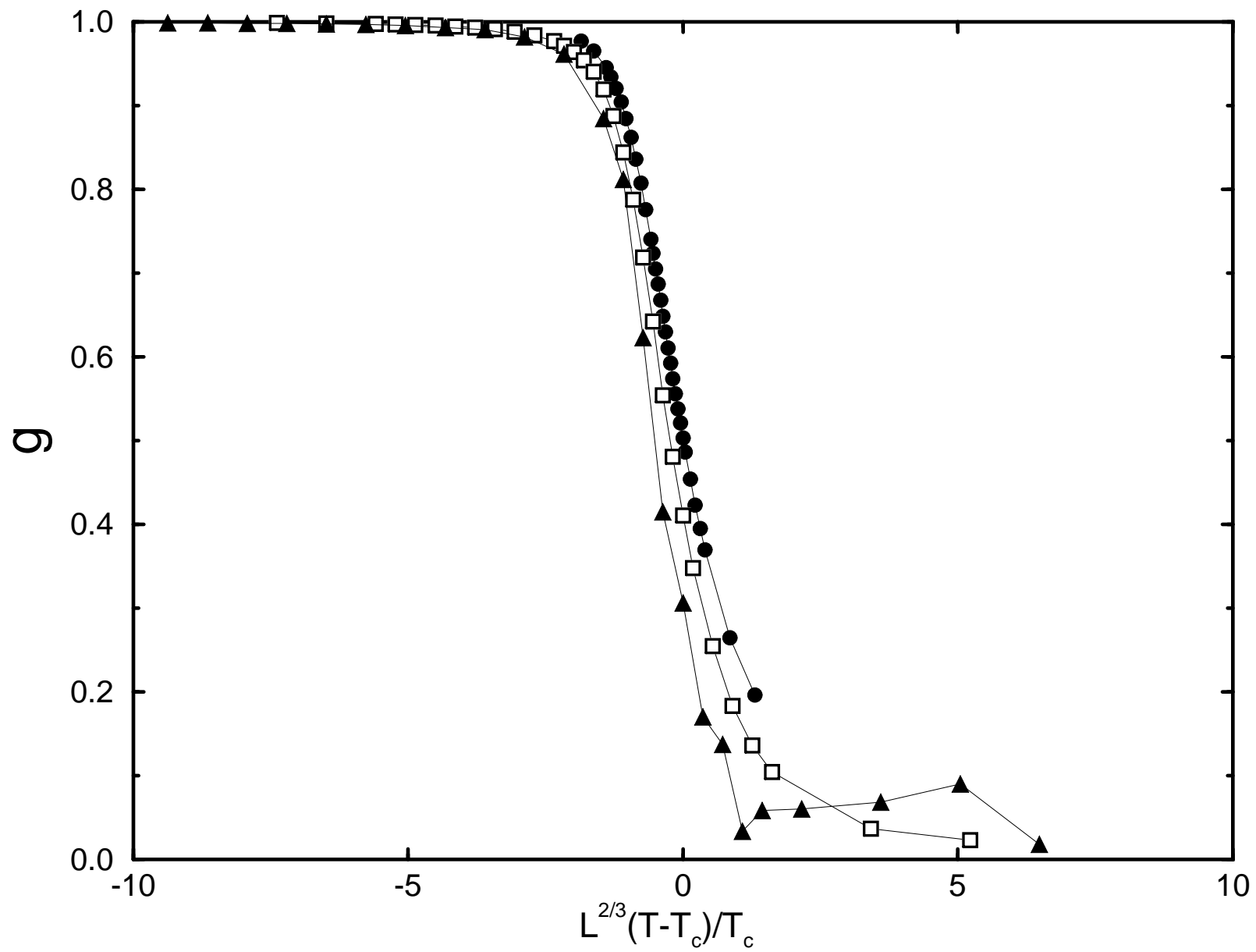
References

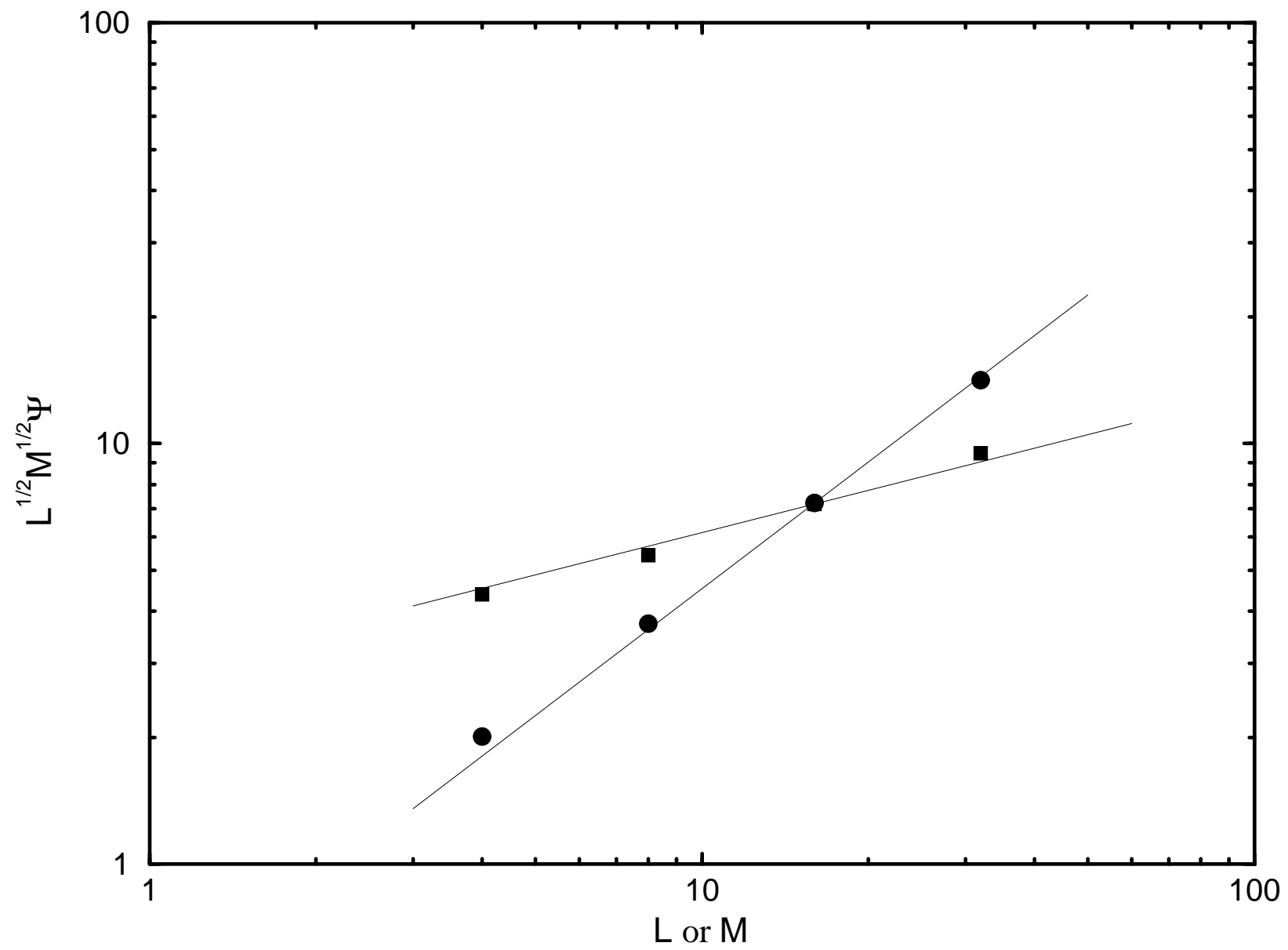
1. S. Katz, J. L. Lebowitz, and H. Spohn, *Phys. Rev. B* **28**:1655 (1983).
2. S. Katz, J. L. Lebowitz, and H. Spohn, *J. Stat. Phys.* **34**:497 (1984).
3. H. van Beijeren and L. S. Schulman, *Phys. Rev. Lett.* **53**:806 (1984).
4. For reviews, see B. Schmittmann, *Int. J. Mod. Phys.* **4**:2269 (1990); B. Schmittmann and R. K. P. Zia, in *Phase Transitions and Critical Phenomena*, edited by C. Domb and J. L. Lebowitz (Academic Press, New York, in press).
5. H. K. Janssen and B. Schmittmann, *Z. Phys. B* **64**:503 (1986).
6. K.-t. Leung and J. Cardy, *J. Stat. Phys.* **44**:567 (1986).
7. J. L. Vallés and J. Marro, *J. Stat. Phys.* **49**:89 (1987).
8. A. Achahbar and J. Marro, *J. Stat. Phys.*, in press (1994).
9. K.-t. Leung, *Phys. Rev. Lett.* **66**:453 (1991).
10. K.-t. Leung, *Int. J. Mod. Phys. C* **3**:367 (1992).
11. N. Ito, *Int. J. Mod. Phys. C* **4**:525 (1993).
12. K. Binder and J.-S. Wang, *J. Stat. Phys.* **55**:87 (1989).
13. E. L. Praestgaard, H. Larsen, and R. K. P. Zia, *Europhys. Lett.* **25**:447 (1994).
14. J.-S. Wang, K. Binder, and J. L. Lebowitz, *J. Stat. Phys.* **56**:783 (1989).

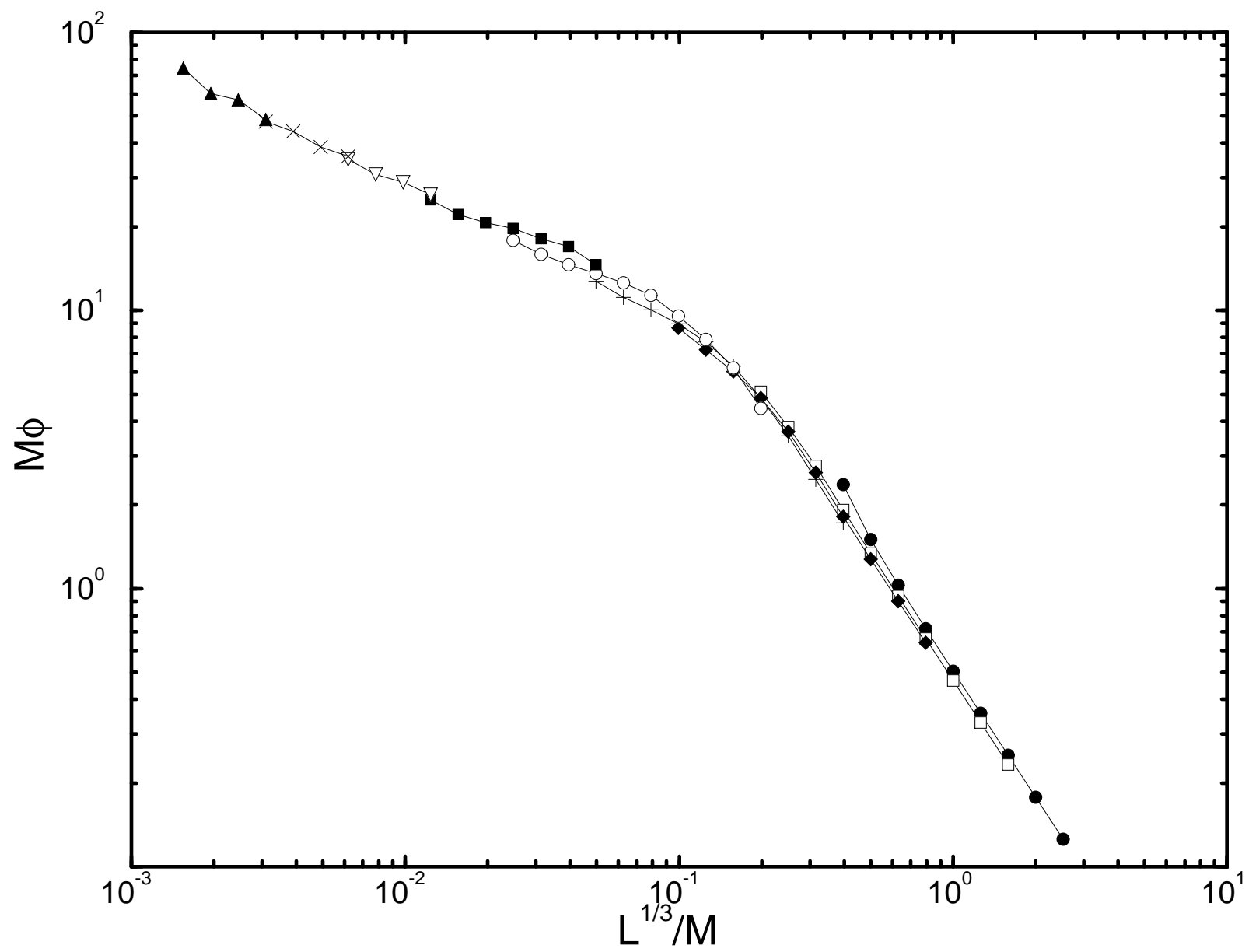
Figure Captions

- Fig. 1.** The locations of the susceptibility peaks plotted against $L^{-2/3}$, for rectangular systems with $S = 2^{-10/3}$ (diamonds, $M = 32, 64$), $S = 1/8$ (squares, $M = 16, 32, 64$), $S = 2^{-8/3}$ (circles, $M = 16, 32, 64$), $S = 1/4$ (triangles, $M = 16, 32$), and for the square systems (pluses, $M = 32, 64, 128, 256$).
- Fig. 2.** The fourth-order cumulant g against scaling variable $L^{2/3}(T - T_c)/T_c$, here $T_c = 1.41$. The system sizes are 16×16 (circles), 128×32 (squares), and 1024×64 (triangles).
- Fig. 3.** Limiting behavior of the order parameter at T_c . Circles are for $L \rightarrow \infty$ and squares are for $M \rightarrow \infty$. The straight lines have slopes 1 and $1/3$, respectively.
- Fig. 4.** Scaling plot of the order parameter at the critical point, $T_c = 1.41$. Each set of data has a fixed M value, $M = 4$ (solid circles), $M = 8$ (open squares), $M = 16$ (diamonds), $M = 32$ (pluses), $M = 64$ (open circles), $M = 128$ (squares), $M = 256$ (open triangles), $M = 512$ (crosses), $M = 1024$ (up triangles).
- Fig. 5.** Scaling plot of the susceptibility at the critical point, $T_c = 1.41$. The symbols are the same as in Fig. 4.
- Fig. 6.** Scaling plot of the fourth-order cumulant at the critical point. The symbols are the same as in Fig. 4.
- Fig. 7.** Scaling plot of the order parameter away from critical point. The system sizes are 16×16 (circles), 128×32 (open squares), and 1024×64 (triangles).
- Fig. 8.** Order parameter to some power, Ψ^2 (circles) and $\Psi^{10/3}$ (squares), versus temperature T . The system size is 1024×64 .
- Fig. 9.** Scaling plot of the susceptibility χ' above the critical temperature. The system sizes are 8×16 (circles), 64×32 (open squares), and 512×64 (triangles).









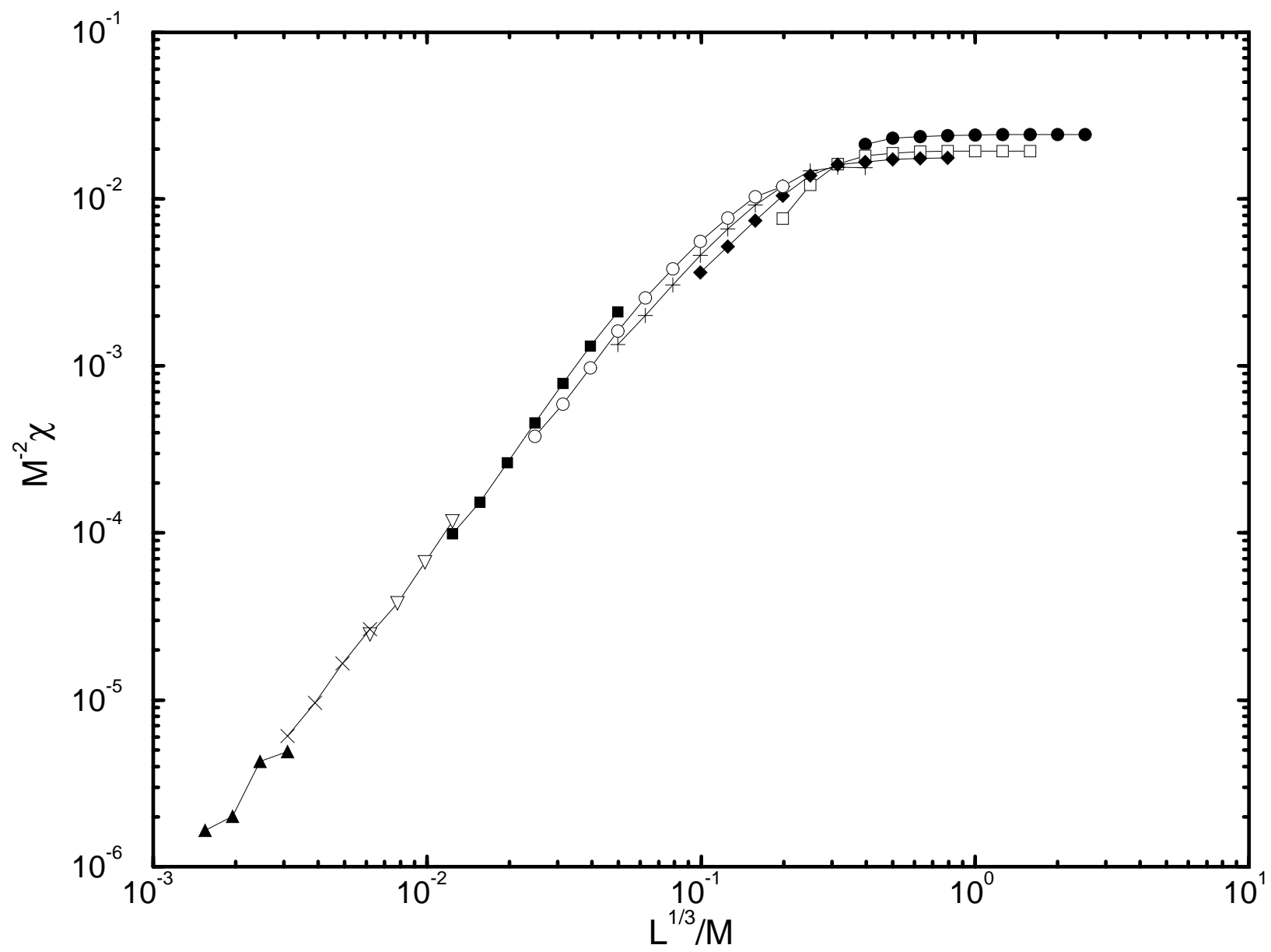


Fig. 6, J-S Wang

